European Conference on Computational Fluid Dynamics
ECCOMAS CFD 2006
P. Wesseling, E. Oñate, J. Périaux (Eds)

MULTIDISCIPLINARY DESIGN OPTIMIZATION OF WING SHAPE WITH NACELLE AND PYLON

Takayasu Kumano *, Shinkyu Jeong, Shigeru Obayashi,

Yasushi Ito †, Keita Hatanaka ††, and Hiroyuki Morino

* Institute of Fluid Science, Tohoku University,
Sendai 980-8577, Japan
e-mail: kumano@edge.ifs.tohoku.ac.jp
Web page: http://www.ifs.tohoku.ac.jp/edge/

†University of Alabama at Birmingham,
1530 3rd AVE S, Birmingham, AL 35294-4461, USA
e-mail: yito@uab.edu
Web page: http://www.dpo.uab.edu/~yito/

††Mitsubishi Heavy Industries, Ltd.,
Nagoya 455-8515, Japan

Key words: MDO, CFD, CSD, Kriging Model, MOGA, SOM, ANOVA

Abstract. *A Multidisciplinary Design Optimization (MDO) system for a wing with nacelle and pylon is developed. The present MDO system is based on the integration of Computational Fluid Dynamics (CFD) codes and NASTRAN based an aeroelastic-structural interface code. The Kriging model is employed to save the computational time of objective function evaluations in Multi-Objective Genetic Algorithm (MOGA). In the present multi-objective optimization, aerodynamic optimization is performed to minimize the drag and the shock wave strength at inboard of pylon, and structural optimization is performed to obtain the minimum wing weight with the constraints of flutter and strength. As a result of the optimization, several solutions improved in all objective function values compared with the baseline shape have been obtained. Furthermore, features of the design space have been investigated by data mining techniques using Self-Organizing Map (SOM) and ANalysis Of VAriance (ANOVA).*

1 INTRODUCTION

A conventional aircraft design has focused on an aerodynamic performance and auxiliary design revisions have been done to satisfy other design requirements from the structure and system. However, based on such an aerodynamically oriented design process, it is difficult to design the aircraft considering interdisciplinary trade-off, which is particularly remarkable between aerodynamic (minimum drag) and structural (minimum weight) performances. Therefore, researches of MDO for a realistic aircraft design have been conducted by

industries and universities [1-3].

In Japan, a 5-year R&D project has been in progress toward the development of environmentally friendly high performance regional jet aircraft under auspices from New Energy Development Organization of Japan (NEDO) since 2003 [4]. In the project, several research programs have been investigated by industry-government-university cooperation [5]. The conceptual image of a regional jet aircraft is shown in Fig. 1. For the success of the project, a practical MDO system for regional jet wing design is required.

An MDO system was developed for a clean wing under the project [6]. The MDO system is based on the integration of Computational Fluid Dynamics (CFD) codes and the NASTRAN-based aeroelastic-structural interface code. Moreover, the Kriging model is employed to reduce computational expenses for function evaluations in MOGA.

In this work, the MDO tool has been extended to an engine-airframe integration problem which is one of the most important issues in the aircraft design. Shock wave generated at inboard of pylon may lead to the separation and buffeting (Fig. 2). In order to prevent these phenomena, the wing shape near the pylon has been optimized. In the engine-airframe integration system, modification of the geometry is the bottleneck because of complexities at junctions among wing, fuselage, pylon, and nacelle. The automated mesh generator developed in the previous system has been extended for this complicated geometry.

Figure 1. Environmentally friendly high performance regional jet aircraft.

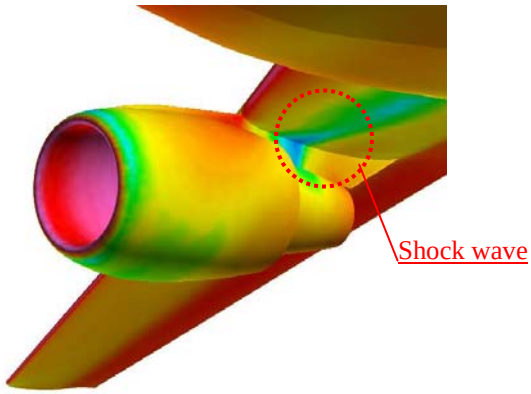

Figure 2. Surface pressure distribution near the nacelle-pylon at the cruising condition.

2 MDO STSTEM

Flowchart of the MDO system extended to an engine-airframe integration problem is shown in Fig. 3. This MDO system consists of three modules: the mesh generation module, CFD & CSD module, and Kriging model & Optimization module.

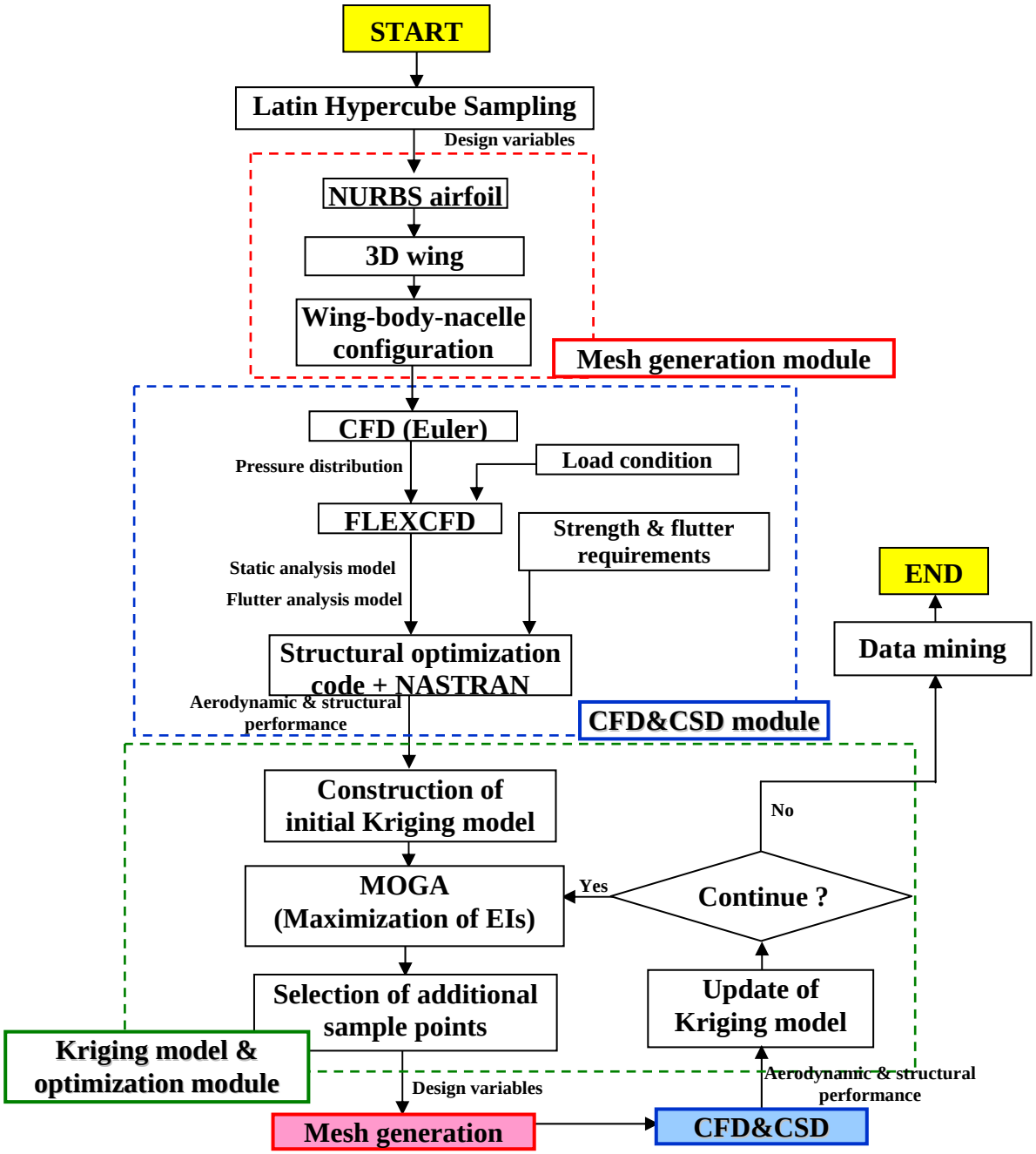

Figure 3. Flowchart of the MDO system for engine-airframe integration problem.

2.1 Mesh Generation Module

In this study, NURBS [7, 8] (Fig. 4) technique employing the B-spline function is adopted. A total number of the design variables is 26. This number was determined as results of comparisons with PARSEC [9]. Especially, NURBS has higher degree of freedom than PARSEC near the leading and trailing edges.

A speedy and robust surface mesh generation system which is applicable to engine-airframe integration is necessary. Although the unstructured dynamic mesh method is very useful for the modification of the wing shape [10], this method sometimes produces the distorted mesh for a large displacement. Furthermore, In the case of the engine-airframe integration, this method cannot be applied because of complexities at junctions among wing, fuselage, pylon, and nacelle. In this study, wing-body-nacelle-pylon configuration mesh is automatically generated in the following steps (Fig. 5).

(a) Airfoil sections are defined by NURBS specified by the design variables.

(b) 3D wing is generated using the airfoil sections.

(c) Extract the intersection lines among wing, fuselage, and nacelle-pylon.

(d) Delete the extra wing and pylon geometries which are inside of other geometies.

(e) Combine the wing, the body, and the nacelle-pylon.

(f) Specify mesh point distributions along ridge lines.

(g) Generate unstructured surface mesh using the advancing front method of TAS-Mesh [11, 12].

(h) Generate unstructured volume mesh using delaunay tetrahedral meshing [13].

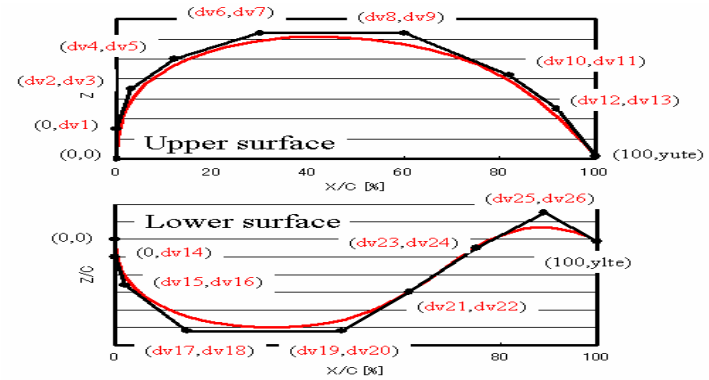

Figure 4. Airfoil defined by NURBS.

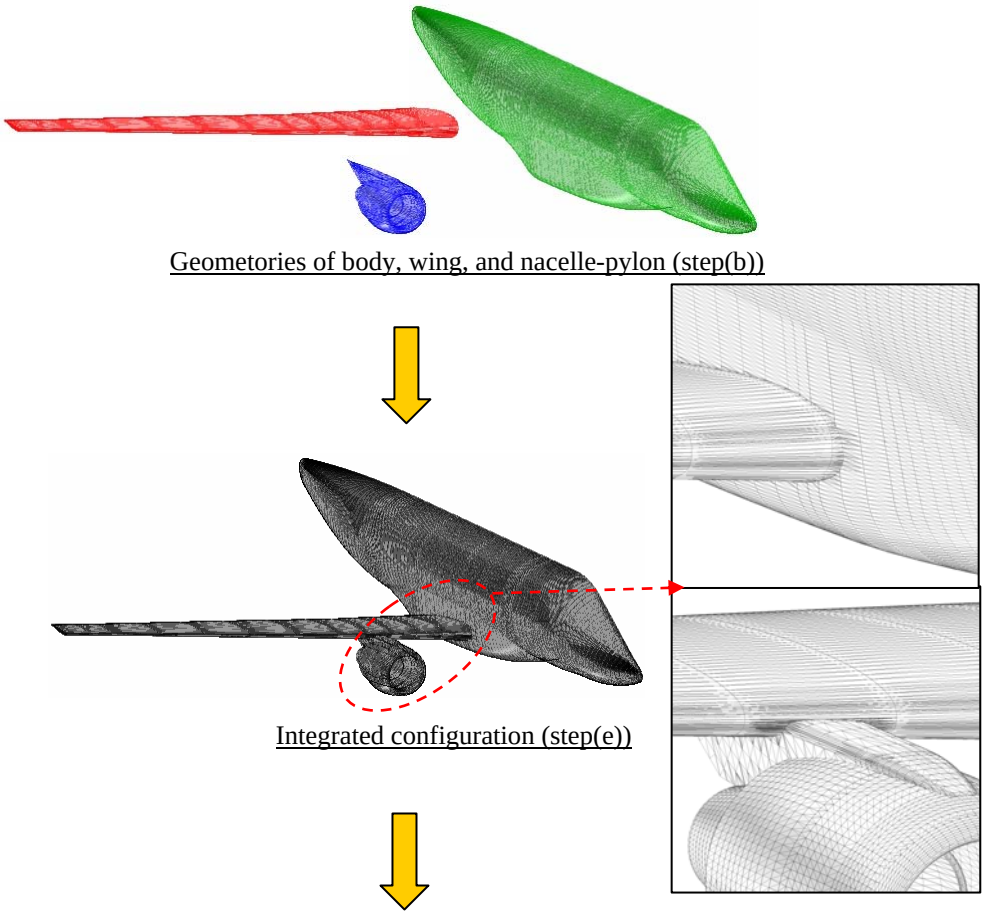

Geometories of body, wing, and nacelle-pylon (step(b))

Integrated configuration (step(e))

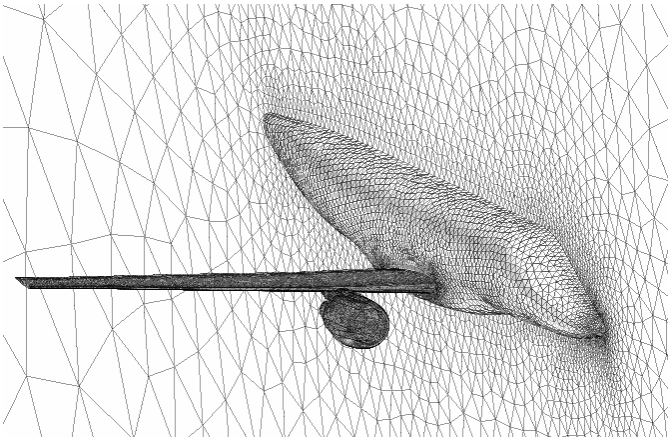

Unstructured surface mesh (step(g))

Figure 5. Procedures for mesh generation.

2.2 CFD & CSD Module

In order to evaluate aerodynamic and structural performances, CFD&CSD module in Fig. 3 is performed. The procedure is as follows:

(a) Euler analysis is performed for the sample points.

(b) Using the pressure distribution obtained from the Euler analysis, structural and flutter analysis models are generated by FLEXCFD which is an aeroelastic-structural interface code.

(c) Structural optimization is conducted to minimize wing weight under the strength and flutter constraints.

Figure 6 shows the CFD (unstructured) and CSD (structured) meshes. In the CFD&CSD module, structural optimization of a wing box is performed to realize minimum weight with constraints of strength and flutter. Given the wing outer mold line for each individual, the finite element model of wing box is generated automatically by the FEM generator for the structural optimization. The wing box model mainly consists of shell elements representing skin, spar and rib. Other wing components are modeled using concentrated mass elements. In the present study, MSC. NASTRAN [14] which is a high-fidelity commercial software is employed for the structural and aeroelastic evaluations.

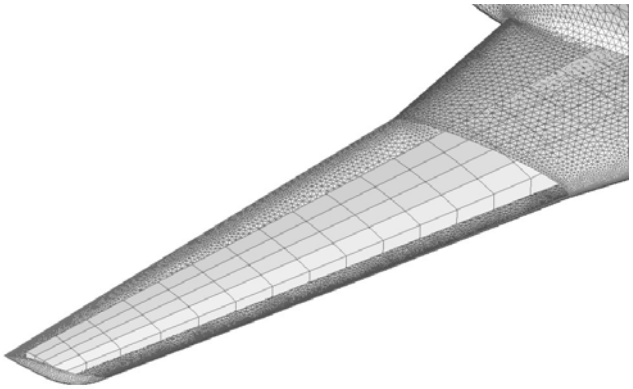

Figure 6. CFD and CSD meshes.

2.3 Kriging Model & Optimization Module

Aerodynamic optimization using MOGA requires a tremendous computational time for objective function evaluations, even with a high performance supercomputer facility. To make the optimization more practical, an approximation model is introduced. The approximation model used in this study is the Kriging model [15, 16]. This model, developed in the field of

spatial statistics and geostatistics, predicts the distribution of function values at unknown points instead of the function values themselves. From the distribution of function values, both function values and their uncertainty at unknown points can be estimated as shown in Fig. 7. By using these values, the balanced local and global search is possible. This concept is expressed as the criterion 'Expected Improvement (EI)' [17]. EI indicates the probability being superior to the current optimum in the design space. By selecting the maximum EI point as an additional sample point for the Kriging model, the improvement of the model accuracy and the exploration of the optimum can be achieved at the same time.

In this research, drastic reduction of computational cost has been realized by replacing the time-consuming high fidelity CFD&CSD solvers with the Kriging approximation models. The overall optimization procedure using the Kriging model is shown in Fig. 8:

(a) Initial sample points distributed uniformly in the design space are selected by the Latin Hypercube Sampling [18].

(b) CFD&CSD module is performed for the initial sample points, and the initial Kriging models are constructed for all objective functions, respectively.

(c) MOGA operations are performed on the Kriging models as
- Generation of initial population
- Evaluation of EI for each objective function
- Selection of parents
- Crossover and mutation
- Evaluation of new individuals
- Evolution for 100 generations
- Selection of additional sample points from non-dominated solutions in terms of EIs

(d) Kriging model is reconstructed as
- Evaluation of the additional sample points with CFD&CSD module
- Update of the Kriging model using all sample points

(e) Go back to (c)

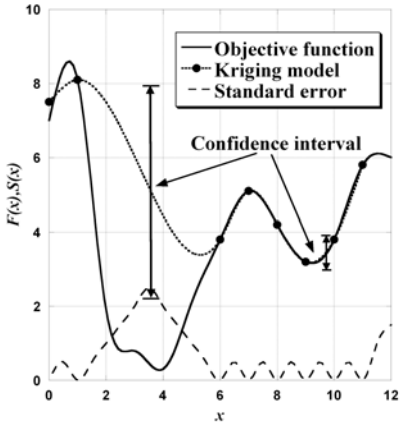

Figure 7. Predicted value and the standard error of the Kriging model.

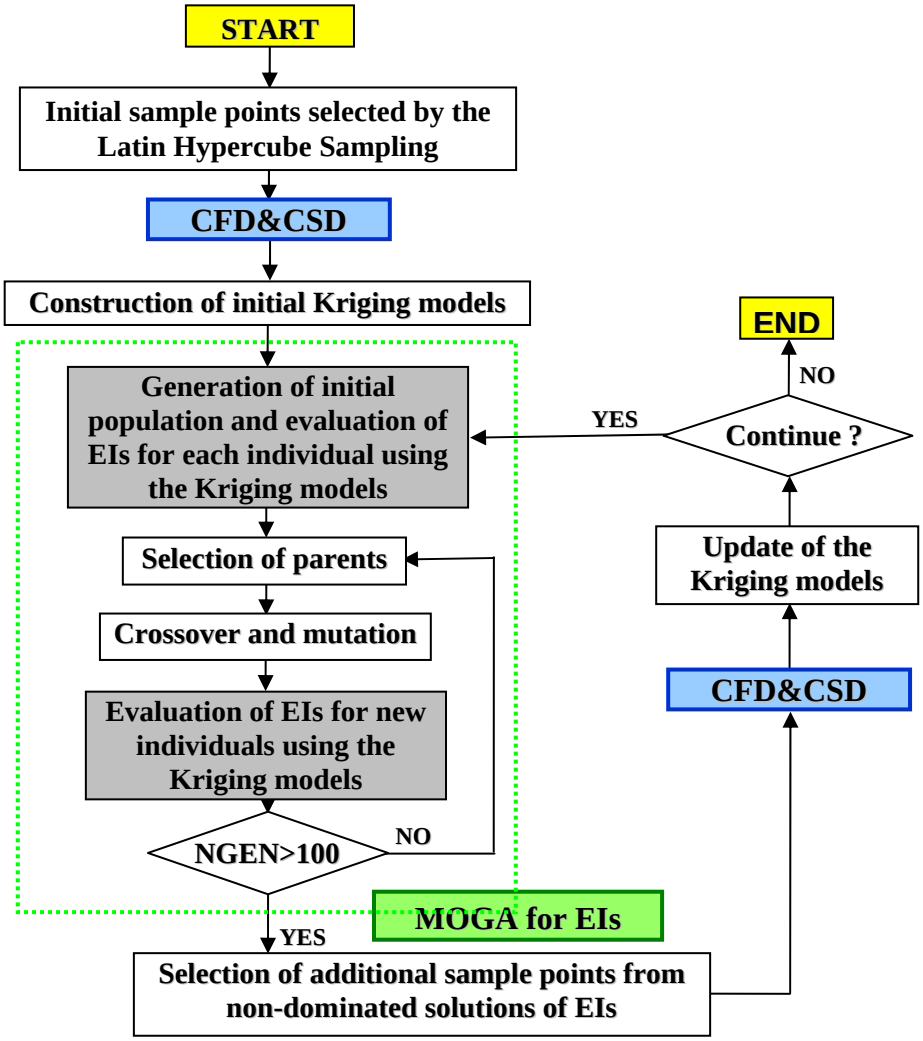

Figure 8. Flowchart of Kriging model & optimization module.

3 OPTIMIZATION PROBLEM

3.1 Definition of Optimization Problem

<Objective functions>

Minimize

- Drag at the cruising condition (C_D).
- Shock strength near wing-pylon junction ($-C_{p,max}$).
- Structural weight of the main wing (Wing weight).

Figure 9 shows the pressure distribution at lower surface of the wing near wing-pylon junction, and $-C_{p,max}$ is defined as indicated.

<Design variables>

- Airfoil shapes of lower surface at 2 span wise sections = 26 variables
- Twist angles at 4 sections = 4 variables

30 variables in total

<Constraints>

- Wing thickness > specified values
- Rear spar heights > specified values
- Strength margin > specified values
- Flutter margin > specified values

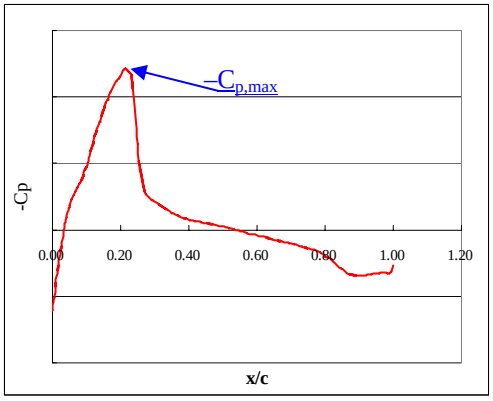

Figure 9. Pressure distribution near the wing-pylon junction.

3.2 Results

In this optimization, the update of the Kriging models has been performed in six times. In total 149 sample points were used. Figure 10 shows performances of the baseline configuration and those of additional sample points at every iteration. As the iteration progresses, individuals move toward the optimum direction. It means that the additional sample points for update are selected successfully. Several solutions improved in all objective function values compared with the baseline shape have been obtained. One of the solutions is

improved in 7.0 counts in C_D, 0.503 in $-C_{p,max}$, and 21.6 kg in the wing weight compared with the performances of the baseline shape.

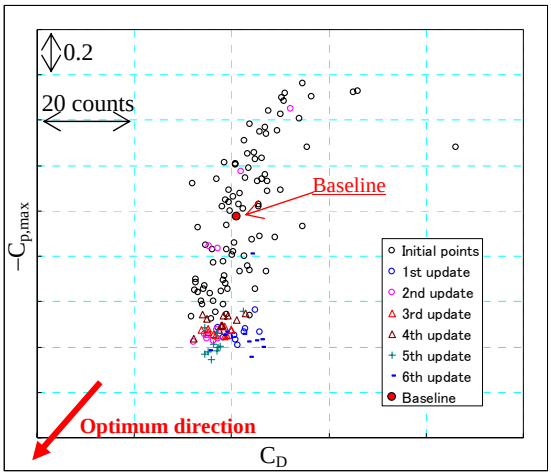

(a) C_D - $-C_{p,max}$

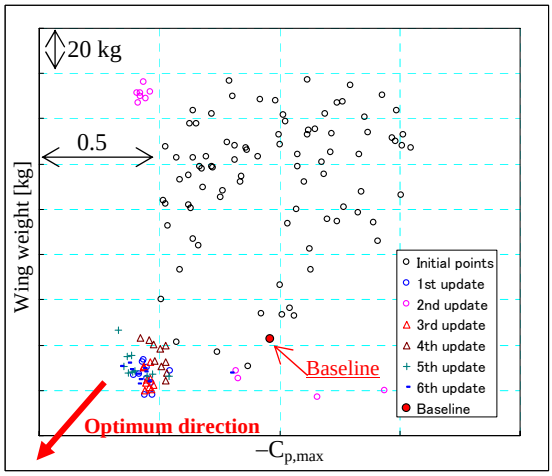

(b) $-C_{p,max}$ - Wing weight

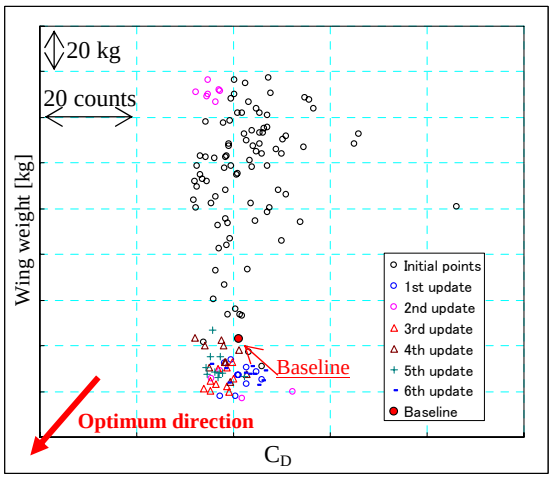

(c) C_D – Wing weight

Figure 10. Performances of baseline shape and sample points.

4 DATA MINING

Data mining is performed by using airfoil parameters different from NURBS because NURBS control points have no significant aerodynamic or structural meaning. Figure 11 shows the airfoil parameters of interest. XmaxL represents a distance from the leading edge to the maximum thickness point of the lower half of the airfoil. maxL is the corresponding maximum thickness of the lower half. XmaxTC is a distance from the leading edge to the maximum thickness point. maxTC is the corresponding maximum thickness. And, sparTC is the thickness at the front spar. These parameters are taken at two sections as shown in table 1.

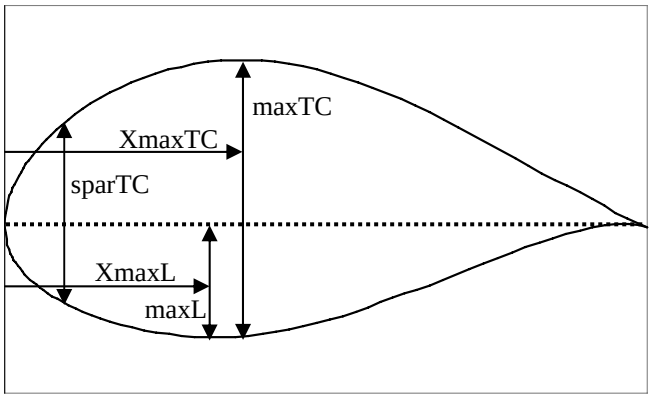

Figure 11. Airfoil parameters using data mining.

Table 1. Airfoil parameters using data mining.

Number	Airfoil parameters
dv1	XmaxL @ η= 0.12
dv2	XmaxL @ η= 0.29
dv3	maxL @ η= 0.12
dv4	maxL @ η= 0.29
dv5	XmaxTC @ η= 0.12
dv6	XmaxTC @ η= 0.29
dv7	maxTC @ η= 0.12
dv8	maxTC @ η= 0.29
dv9	sparTC @ η= 0.12
dv10	sparTC @ η= 0.29

4.1 ANOVA

ANOVA is one of the statistical data mining techniques showing the effect of each design variable to the objective and the constraint functions. ANOVA uses the variance of the model due to the design variables on the approximation function. By decomposing the total variance of the model into the variance due to each design variable, the influence of each design variable on the objective function can be calculated.

Figure 12 shows the results of ANOVA for each objective function. According to the results, dv2, dv7, and dv9 give large influences on C_D. dv6, dv10, and dv2 give large influences on $-C_{p,max}$. Furthermore, dv6, dv8, and dv2 give large influences on the wing weight.

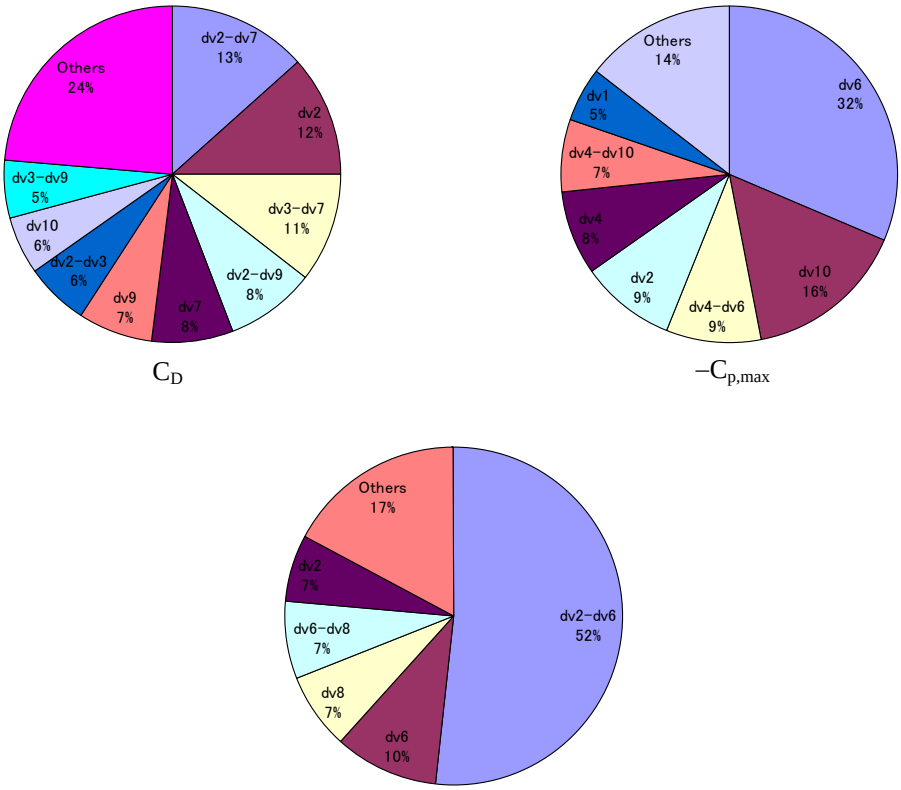

Figure 12. ANOVA results.

4.2 Visualization of Design Space

Next, in order to visualize the design space, Self-Organizing Map (SOM) proposed by Kohonen [19, 20] is employed. This method has been applied to data mining of aerodynamic design space [21-23].

Solutions uniformly sampled from the design space have been projected onto the two-dimensional map of SOM. Figure 13 shows the resulting SOM with 12 clusters considering the three objectives. Furthermore, Fig. 14 shows the same SOMs colored by the three objectives, respectively. These color figures show that the SOM indicated in Fig. 13 can be grouped as follows:

- The upper right corner corresponds to the designs with high wing weight and low C_D.
- The upper edge area corresponds to those with high wing weight.
- The lower right corner corresponds to those with low C_D, $-C_{p,max}$, and wing weight.
- The upper left corner corresponds to those with high C_D.
- The lower left corner corresponds to those with high C_D, and $-C_{p,max}$.

As a result, the lower right corner is the sweet spot in this design space that improves all three objective functions.

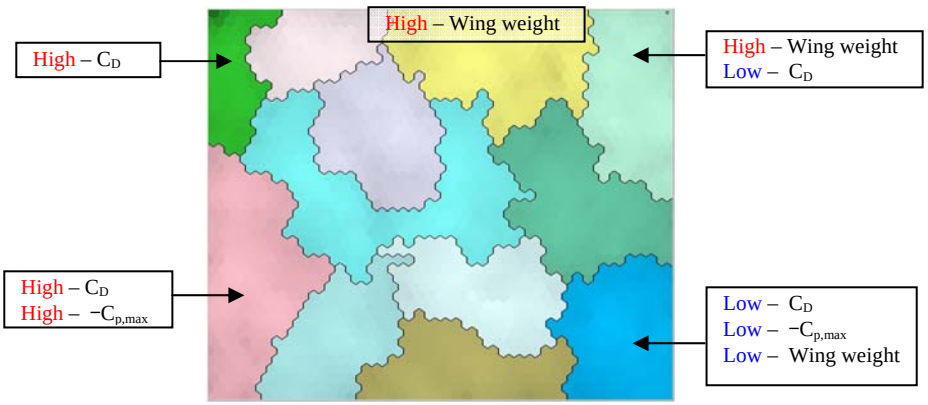

Figure 13. SOM of solutions uniformly sampled from the design space.

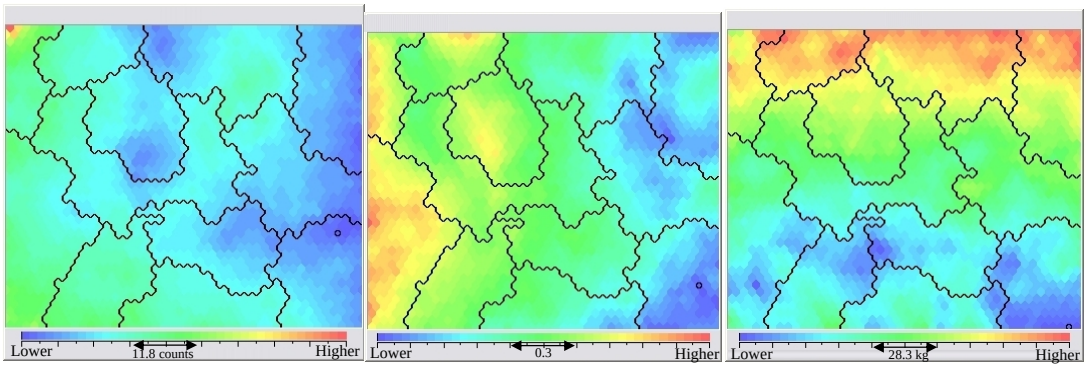

(a) C_D (b) $-C_{p,max}$ (c) Wing weight

Figure 14. SOM of solutions uniformly sampled from the design space colored by the objective functions.

Figure 15 shows the same SOMs colored by four airfoil parameters (dv2, dv6, dv7, and dv10, respectively). In Fig. 15(a) colored by dv2, large dv2 values can be found at the right edge. This area corresponds to small C_D and $-C_{p,max}$ values as shown in Figs. 14(a) and 14(b), respectively. This means that large dv2 values lead to high performances of C_D and $-C_{p,max}$. Furthermore, in Fig. 15(c) colored by dv7, low dv7 values can be found at the right edge. This color pattern is very similar to that for C_D. This also means that low dv7 values lead to high performance of C_D.

In Fig. 15(b) colored by dv6, large dv6 values can be found at the right edge. This means that large dv6 values lead to high performance of $-C_{p,max}$. Also, the color pattern of Fig. 15(d) is very similar to that for $-C_{p,max}$. This means that low dv10 values lead to high performance of $-C_{p,max}$. As seen in Fig. 16, large dv6 and low dv10 values lead to mitigate the blockage between the wing and nacelle. Therefore, the shock wave between the wing and nacelle is weakened. Figures 14(b), 15(b), and 15(d) are found to indicate this phenomenon.

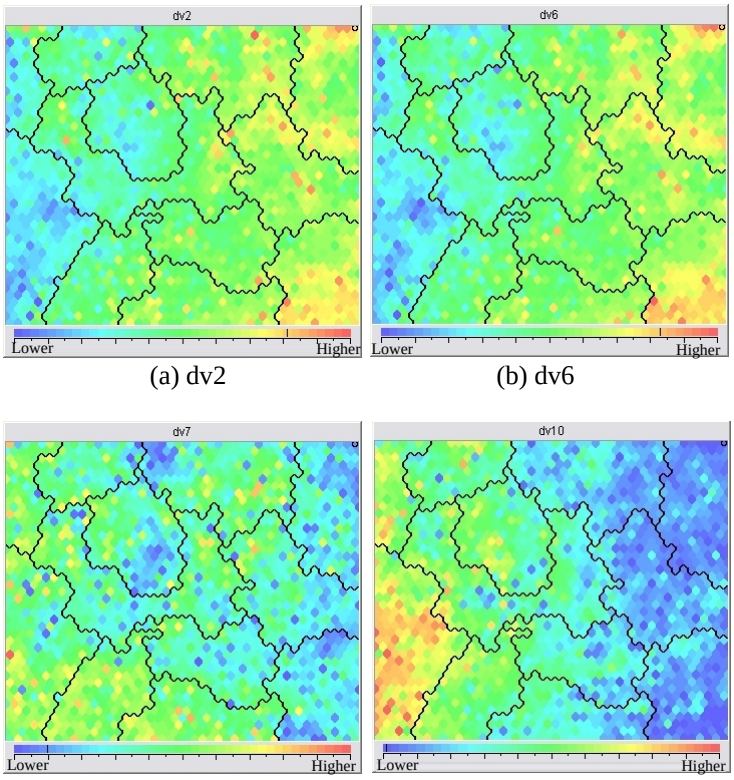

(a) dv2 (b) dv6

(c) dv7 (d) dv10

Figure 15. SOM of solutions uniformly sampled from the design space colored by the airfoil parameters.

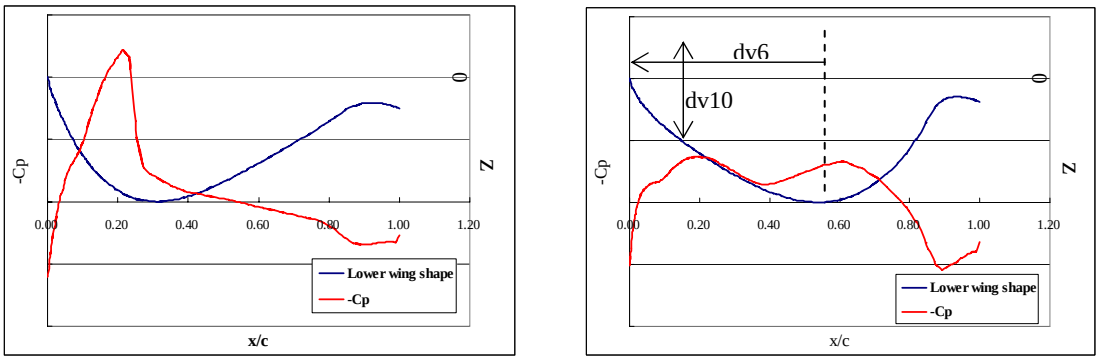

(a) High $-C_{p,max}$ case (c) Low $-C_{p,max}$ case

Figure 16. Pressure distribution near the wing-pylon junction.

4.3 Visualization of Trade-offs

Non-dominated solutions obtained from the final Kriging models have been plotted in the three-dimensional objective function space in Fig. 17 (black points). Blue, red, and green points are the same non-dominated solutions projected onto the two-dimensional objective

function plane. As seen from this figure, there are trade-offs among all objective functions within the sweet spot of the design space.

The same non-dominated solutions have been projected onto the two-dimensional map of SOM. Figure 18 shows the resulting SOM with 13 clusters considering the three objectives. Figure 19 shows the same SOMs colored by the three objectives, respectively. These color figures show that the SOM indicated in Fig. 18 can be grouped as follows:

- The lower right corner corresponds to the designs with high C_D and low $-C_{p,max}$.
- The upper right corner corresponds to the designs with high wing weight.
- The lower left corner corresponds to the designs with low wing weight.
- The upper left corner corresponds to the designs with high $-C_{p,max}$ and low wing weight.

In the lower right corner of Fig. 19(a) and (b), the solutions have maximum C_D and minimum $-C_{p,max}$ solutions. Therefore, there is a strong trade-off between C_D and $-C_{p,max}$.

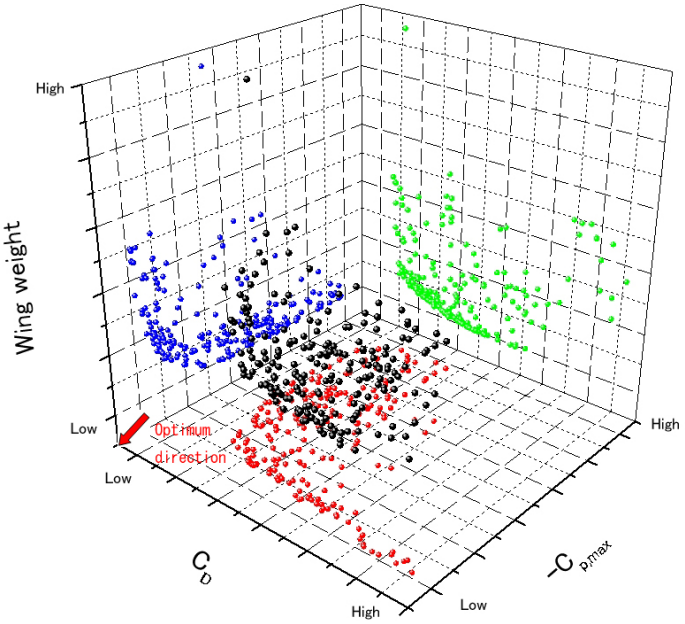

Figure 17. Non-dominated solutions projected onto three-dimensional objective function space.

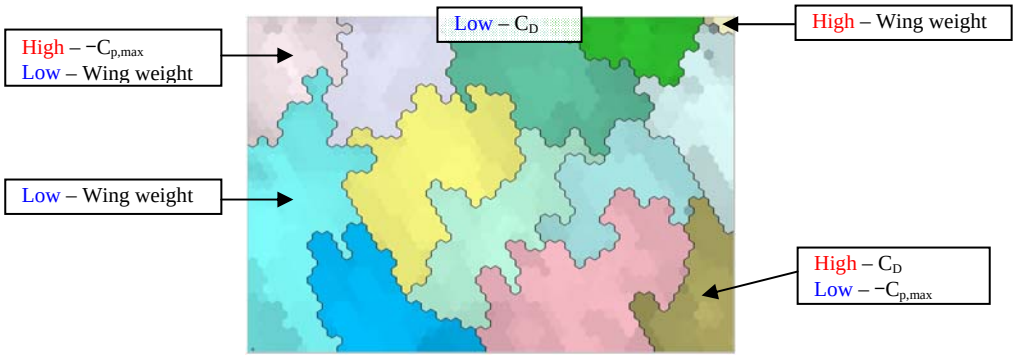

Figure 18. SOM of non-dominated solutions obtained from the Kriging model.

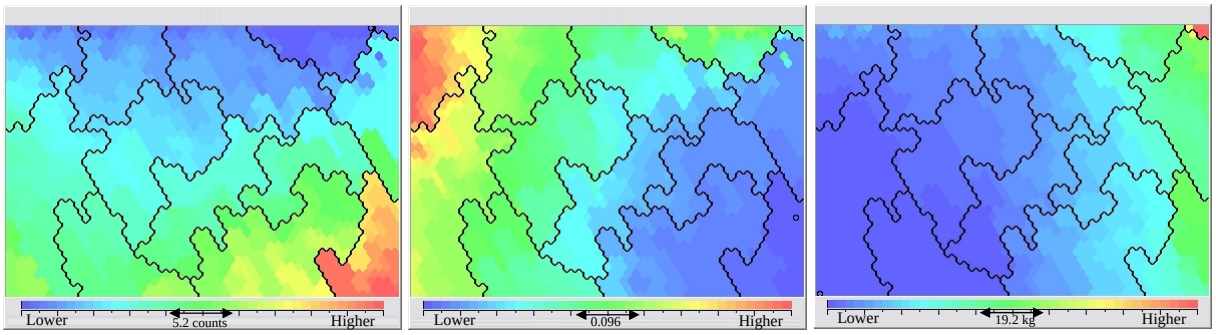

(a) C_D (b) $-C_{p,max}$ (c) Wing weight

Figure 19. SOM of non-dominated solutions colored by the objective functions.

Figure 20 shows the same SOMs colored by six airfoil parameters (dv2, dv4, dv5, dv6, dv8, and dv9, respectively). In Fig. 20(a) colored by dv2, large dv2 values can be found at the lower right corner. This area corresponds to large C_D and small $-C_{p,max}$ values as shown in Figs. 19(a) and (b). This means that dv2 has influence on trade-off between C_D and $-C_{p,max}$. Similarly, in Figs. 19(b)-(d) colored by dv4, dv5, and dv6, respectively, large values can be found at the lower right corner. It means that dv4, dv5, and dv6 also have influence on trade-off between C_D and $-C_{p,max}$. On the other hand, dv8 and dv9 have little influence on the objective functions.

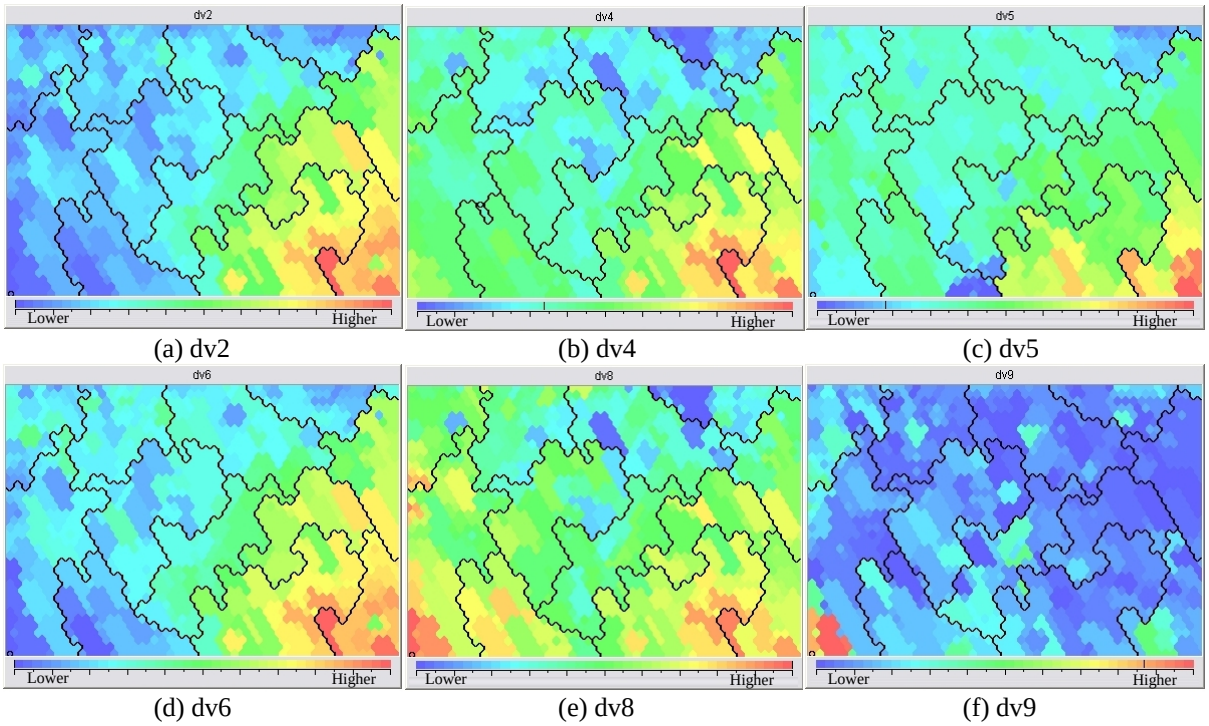

(a) dv2 (b) dv4 (c) dv5

(d) dv6 (e) dv8 (f) dv9

Figure 20. SOM of non-dominated solutions colored by the airfoil parameters.

5 CONCLUSION

The MDO tool has been extended to an engine-airframe integration problem which is one of the most important issues in the aircraft design. The mesh generator developed in the previous system have been improved and made it possible to modify the wing shape automatically in the complicated geometry problem.

The present system has been applied to the wing with nacelle and pylon design problem that considers the aerodynamic and structural performances simultaneously. As a result of the optimization, non-dominated solutions were successfully generated after 149 function evaluations. One of the non-dominated solutions is found to be improved by 7.0 counts in C_D, 0.503 in $-C_{p,max}$, and 21.6 kg in the wing weight compared with the performances of the baseline shape. Therefore, it has been verified that the revised MDO system is very useful and efficient.

Moreover, data mining for the design space was performed using ANOVA and SOMs. In the case of SOM obtained from solutions uniformly sampled from the design space, the sweet spot was found in the design space. Furthermore, as the result of the same SOMs colored by the airfoil parameters and ANOVA, airfoil parameters effective to improve or worsen the objective functions were found.

In the case of SOM obtained from non-dominated solutions on the Kriging model, it was found that there were trade-offs among C_D, $-C_{p,max}$, and wing weight within the sweet spot. As the result of the SOMs colored by the airfoil parameters, particular airfoil parameters having influence on these trade-offs were found.

Data Mining using SOM and ANOVA provides knowledge and valuable information regarding the design space and trade-off, and will extract hidden information during the optimization.

REFERENCES

[1] Kroo, I., Altus, S., Braun, R., Gage, P., and Sobieski, I., "Multidisciplinary Optimization Methods for Aircraft Preliminary Design," AIAA Paper 94-4325-CP, 1994.

[2] Sobieszczanski-Sobieski, J. and Haftka, R. T., "Multidisciplinary Aerospace Design Optimization: Survey of Recent Developments," Structural Optimization, Vol.14, No.1, 1997, pp. 1-23.

[3] Martins, J. R. R. A., Alonso, J. J., and Reuther, J. J., "High-Fidelity Aerostructural Design Optimization of a Supersonic Business Jet," *Journal of Aircraft*, Vol. 41, No. 3, 2004, pp. 523-530.

[4] "NEDO" website, URL:http://www.nedo.go.jp/.

[5] Chiba, K., Obayashi, S., Nakahashi, K. and Morino, H., "High-Fidelity Multidisciplinary Design Optimization of Aerostructural Wing Shape for Regional Jet," AIAA paper 2005-5080, June 2005.

[6] Kumano, T., Jeong, S., Obayashi, S., Ito, Y., Hatanaka, K., and Morino, H., "Multidisciplinary Design Optimization of Wing Shape for a Small Jet Aircraft Using Kriging Model," AIAA paper 2006-0932, 2006.

[7] Lepine, J., Guibault, F., Trepanier, J-Y., and Pepin, "Optimized Nonuniform Rational B-spline Geometrical Representation for Aerodynamic Design of Wings," AIAA Journal, Vol. 39, 2001, pp. 2033-2041.
[8] Takenaka, K., Obayashi, S., Nakahashi, K., Matsushima, K., "The Application of MDO Technologies to the Design of a High Performance Small Jet Aircraft - Lessons learned and some practical concerns -," AIAA paper 2005-4797, June 2005.
[9] Oyama, A., Obayashi, S., Nakahashi, K., and Hirose, N., "Aerodynamic Wing Optimization via Evolutionary Algorithms Based on Structured Coding," Computational Fluid Dynamics Journal, Vol.8, No.4, 2000, pp. 570-577.
[10] Murayama, M., Nakahashi, K., and Matsushima, K., "Unstructured Dynamic Mesh for Large Movement and Deformation," AIAA Paper 2002-0122, 2002.
[11] Yamazaki, W., Matsushima, K., and Nakahashi, K., "Aerodynamic Optimization of NEXST-1 SST Model at Near-Sonic Regime," AIAA Paper 2004-0034, 2004.
[12] Ito, Y. and Nakahashi, K., "Direct Surface Triangulation Using Stereolithography Data," AIAA Journal, Vol. 40, No. 3, 2002, pp. 490–496.
[13] Sharov, D. and Nakahashi, K., "A Boundary Recovery Algorithm for Delaunay Tetrahedral Meshing," Proceedings of the 5th International Conference on Numerical Grid Generation in Computational Field Simulations, 1996, pp. 229–238.
[14] "MSC Software" website, URL: http://www.mscsoftware.com/.
[15] Donald, R. J., Matthias S. and William J. W., "Efficient Global Optimization of Expensive Black-Box Function," Journal of global optimization, Vol.13, 1998, pp. 455-492.
[16] Jeong, S., Murayama, M., and Yamamoto, K., "Efficient Optimization Design Method Using Kriging Model," Journal of Aircraft, Vol.42, 2005, pp. 413-420.
[17] Matthias, S., "Computer Experiments and Global Optimization," Ph.D Dissertation, Statistic and Actuarial Science Dept., University of Waterloo, Waterloo, Ontario, 1997.
[18] Mckay, M. D., Beckman, R. J., and Conover, W. J., "A Comparison of Three Methods for Selecting Values of Input Variables in the Analysis of Output from a Computer Code," Technometric, Vol. 21, No. 2, 1979, pp. 239-245.
[19] Kohonen, T., Self-Organizing Maps, Springer, Berlin, Heidelberg, 1995.
[20] Krzysztof, J. C., Witold, P. and Roman, W. S., *Data Mining Methods for Knowledge Discovery*, Kluwer Academic Publisher, Dordrecht, 1998.
[21] Obayashi, S., Jeong, S., and Chiba, K., "Multi-Objective Design Exploration for Aerodynamic Configurations," AIAA Paper 2005-4666, 2005.
[22] Jeong, S., Chiba, K., and Obayashi, S., "Data Mining for Aerodynamic Design Space," Journal of Aerospace Computing, Information, and Communication, Vol. 2, 2005, pp. 452–469.
[23] Pediroda, V., Poloni, C., and Clarich, A., "A Fast and Robust Adaptive Methodology for Airfoil DesignUnder Uncertainties based on Game Theory and Self-Organising-Map Theory," AIAA paper 2006-1472, 2006.